**RESEARCH**

# Magnetic Iron Oxide Kaolinite Nanocomposite for Effective Removal of Congo Red Dye: Adsorption, Kinetics, and Thermodynamics Studies

Nafis Mahmud[1] · Abdelbaki Benamor[1]

## Abstract

Magnetic iron oxide/kaolinite (MK) composite was synthesized using co-precipitation method and characterized by XRD, FTIR, SEM/EDX, TGA, XPS, VSM, and zeta potential analyses. The synthesized composite consisting of kaolinite halloysites with small clusters of iron oxide on its outer surface was used in batch experiments to adsorb Congo red dye at different temperatures. The adsorption data were fitted to three different isotherms with Langmuir adsorption isotherm best fitting the adsorption data. The maximum adsorption capacity of MK adsorbent was found to be around 45.59 mg/g. Adsorption kinetics data obtained at three different temperatures were fitted to pseudo-first-order and pseudo-second-order models, where the latter model was able to better interpret the obtained kinetics data with a pseudo-second-order rate constant of $8.60 \times 10^{-2}$ g.mg$^{-1}$.min$^{-1}$. Further analysis of the kinetic data revealed that the adsorption mechanism could be explained via intraparticle diffusion model. Thermodynamic parameters $\Delta G°$, $\Delta H°$, and $\Delta S°$ for the adsorption process were determined with the results revealing the adsorption process to be favorable, endothermic, and physical in nature. Finally, comparison with other adsorbents showed that the synthesized MK composite exhibits significant potential to be used as an adsorbent for the removal of organic pollutants from aqueous solutions.

**Keywords** Kaolinite · Iron oxide · Nanocomposite · Adsorption · Congo red dye

## Introduction

Water pollution triggered from industrial waste discharge has become a growing concern for countries worldwide [1, 2]. Preservation of water is crucial for the safety and well-being of both human and aquatic life. Huge volumes of wastewater are being directly discharged to the water bodies without any prior treatment. A large percentage of the industrial waste consists of organic dyes coming mainly from their extensive use in textile, tannery, paper, and printing industries. Organic dyes are known to be extremely harmful to human health as they are toxic and carcinogenic as well [3]. They can inhibit the light from going into the aquatic system and disrupt the photosynthesis process [4]. Therefore, developing efficient methods to remove these harmful dyes from the industrial wastewater is very crucial.

Various techniques have been employed to remove dyes from wastewater, including adsorption, photocatalysis, coagulation, flocculation, ion exchange, electro chemical method, chemical oxidation, and aerobic and anaerobic degradation using microbes [3, 5–7]. Among these techniques, adsorption is a commonly employed technique as it is easy to operate, highly efficient, and inexpensive compared to the other methods. The adsorption process is largely dependent on the nature and type of the adsorbent being used. Various adsorbents like activated carbon, metal oxides, polymers, and zeolites have been applied to remove dyes from wastewater [2, 8–10]. However, the different studied adsorbents available in the open literature have several drawbacks such as low sorption capacity, high production, and recovery problems. Therefore, development of easily recoverable adsorbents with high sorption capability and low cost is very crucial for their industrial application.

Clay minerals are gradually becoming promising adsorbents for removal of dye pollutants from industrial water effluents due to their non-toxicity, low cost, easy availability, and affinity for dyes [11]. They are unique materials that are phyllosilicates in nature possessing high surface

✉ Abdelbaki Benamor
benamor.abdelbaki@qu.edu.qa

[1] Gas Processing Centre, College of Engineering, Qatar University, 2713 Doha, Qatar

area and ion exchange capabilities [12]. They exist in several forms in nature such as alunite, smectite, kaolinite, bentonite and several others [13]. Of these, kaolinite is the most abundant and commonly used in rubber, ceramics, and cosmetics industries [14]. Kaolinite minerals are non-toxic and cheaper adding more values to their potential of use as adsorbent over the conventional adsorbents [15]. However, several studies showed that the adsorption capability of kaolinite is significantly lower than commercial adsorbent as they are inactive in nature and possess low surface area [16]. Furthermore, recovery of used kaolinite adsorbents for cyclic use still remains a challenge. Therefore, it is necessary to modify the kaolinite surface to achieve satisfactory dye removal and ensuring a good recovery of the adsorbent for further use. A common way of improving the performance of clay minerals is through surface modifications. The surface of the kaolinite minerals can be modified by surfactants (didodecyldimethylammonium bromide) [17], polymers (2-acrylamido-2-methylpropane sulfonic acid) [18], and acids activation (sulfuric acid, $H_2SO_4$) [19].

It is expected that using magnetic iron oxide or $Fe_3O_4$ nanoparticles to modify the surface kaolinite clay minerals will result in significant improvement in dye removal while ensuring the recovery of the adsorbent, simultaneously. $Fe_3O_4$ are environmentally benign, low cost, biocompatible, and magnetically recoverable and have been widely used to modify and improve several adsorbents [20–22]. Owing to these favorable properties, it is expected that incorporating $Fe_3O_4$ or iron oxide with kaolinite mineral may well result in the formation of an efficient and recoverable composite. Therefore, in this study, magnetic iron oxide/kaolinite composite were prepared via co-precipitation method and characterized using X-ray diffraction (XRD), Fourier-transform infrared spectroscopy (FTIR), scanning electron microscopy with energy dispersive x-ray spectroscopy (SEM/EDX), thermogravimetric analysis (TGA), X-ray photoelectron spectroscopy (XPS), scanning electron microscopy (SEM), and vibrating sample magnetometer (VSM) and zeta potential techniques. Congo red (CR) an anionic dye with azo molecular structure was selected as a model pollutant and the effect of pH, adsorbent dosage, contact time, and initial dye concentration on its adsorptive removal from aqueous solution using MK composite was investigated. Moreover, adsorption isotherms, kinetics, and thermodynamic studies were also conducted. Results obtained from these studies can provide useful insight on the design and development of low-cost clay, highly magnetic and iron oxide-based adsorbents that can be effectively used to remove Congo red dye and hopefully other recalcitrant organic pollutants from wastewater effluents.

## Materials and Methods

### Chemicals

$FeCl_2.4H_2O$ and $FeCl_3.6H_2O$ both of purity 99%, 25% $NH_4OH$, NaOH (Purity 98%), and HCl (Purity 35–38%) were obtained from ResearchLab. Absolute ethanol (purity 99.9%) and natural kaolinite were purchased from Scharlau and Sigma-Aldrich, respectively. Deionized water was used for preparation and cleaning of the composites throughout the experiments. All the chemicals were used without any further purification.

### Preparation of Magnetic Iron Oxide/Kaolinite Composite

A facile co-precipitation method was used to synthesize magnetic iron oxide/kaolinite composite [23]. Firstly, 1 g of kaolinite was dissolved in 60 mL of deionized water and stirred for 15 min at 60 °C. Next, around 0.0045 mol of $FeCl_2.4H_2O$ and 0.0048 mol of $FeCl_3.6H_2O$ were added and the solution was further stirred under $N_2$ atmosphere for 15 min. Afterwards, around 6 mL of 25% $NH_4OH$ solution was added to adjust the solution pH to 10. The temperature of the solution was then reduced to 50 °C and the solution was stirred for three additional hours. Finally, the precipitate obtained was separated using a magnet and cleaned in multiple cycles of DI water and ethanol and dried at 60 °C under vacuum. Finally, a magnetic iron oxide/kaolinite composite was obtained which was used as an adsorbent in this work.

### Adsorbent Characterization

The X-ray diffraction (XRD) patterns of the magnetic iron oxide/kaolinite (MK) adsorbents were measured using a PAN analytical X-ray diffractometer (Model: EMPYREAN), operated at 40 kV using a Cu Kα radiation (λ = 1.5406 Å) within a range of 5 to 90°. The FT-IR spectra of MK were recorded using Thermo Scientific Nicolet iS10 in a wavelength range of 4000–500 $cm^{-1}$ in transmittance mode at room temperature. The morphology and elemental composition of the MK adsorbents were determined using a FEI scanning electron microscopy (model: Nova Nano SEM 450) with Bruker EDX detector. Thermogravimetric analysis (TGA) of the composite was carried out in a Perkin Elmer thermogravimetric analyzer (model: Pyris 1). For this purpose, powdered samples of MK were placed on a platinum pan and heated at a temperature range of 25–900 °C at rate of 5 °C.$min^{-1}$ under $N_2$ atmosphere. An X-ray photoelectron spectroscopy (XPS) analysis of the sample was also

conducted on an AXIS Ultra DLD, KRATOS XPS apparatus. Finally, vibrating sample magnetometer (model: Lakeshore 7404) was used to investigate the magnetics properties of the composite at room temperature.

## Adsorption Experiments

Batch adsorption experiments were performed to investigate the effect of various operating parameters such as pH, adsorbent dose, and initial dye concentration on the adsorption of the Congo red dye. The pH experiments were performed on 50 mL of Congo red dye solution of fixed concentration (20 mg.L$^{-1}$) at fixed adsorbent dosage of 1.0 g.L$^{-1}$ by adjusting the pH to the desired value using 0.1 M HCl or NaOH solutions at 303 K. Similarly, the effect of adsorbent dosage and initial dye concentration on the adsorption performance was also investigated by varying the amount of adsorbent and dye concentrations, respectively. Adsorption isotherm studies were conducted by adding 1.0 g.L$^{-1}$ of the as-prepared MK adsorbents to a series of 100-mL conical flasks containing 50 mL Congo red dye solutions of different concentrations (20–90 mg/L) at pH 5.5. The flasks were then sealed and stirred at 200 RPM in a Labnet air bath shaker for 2 h at different temperatures (303, 313, and 323 K). After the completion of the adsorption experiments, the MK adsorbents were then separated magnetically and the Congo red dye concentrations in the supernatant was measured by determining the maximum absorbance at 498 nm using HACH UV/Vis spectrophotometer (model: DR 3000). The amount of Congo red adsorbed by the MK adsorbent at equilibrium was determined using the following equation:

$$q_e = \frac{(C_o - C_e)V}{m} \tag{1}$$

where, "$q_e$" represents the amount of Congo red dye adsorbed per gram of the adsorbent, the term "V" stands for the volume of Congo red solution, and "m" represents the mass of the adsorbent, while "$C_o$" and "$C_e$" represent the initial and equilibrium concentrations of the Congo red dye, respectively, and the terms $V$ and $W$ stands for the volume of the solution and mass of the adsorbent. The removal efficiencies were also calculated using the following equation:

$$Removal\ \% = 100 \times \frac{(C_o - C_e)}{C_0} \tag{2}$$

The effect of time on the adsorption process was investigated by performing adsorption kinetics experiments. For this purpose, adsorption experiments were conducted on fixed concentration of Congo red dye (20 mg.L$^{-1}$) with fixed MK dose (1.0 g.L$^{-1}$) at different temperatures (303, 313, 323 K). The samples of dye were taken at pre-set times and their absorbance was measured immediately. Using 'C$_t$' as

the term representing the concentration of Congo Red dye solution remaining at certain time, Eq. (1) can be rewritten to determine the amount of Congo Red dye adsorbed per gram of the adsorbent at that time (q$_t$) using the following equation:

$$q_t = \frac{(C_o - C_t)V}{m} \tag{3}$$

## Results and Discussion

### Characterization

#### XRD Analysis

The crystalline structure and phase composition of the pure kaolinite and as-prepared magnetic iron oxide/kaolinite composite was analyzed using XRD apparatus. As shown in Fig. 1, the XRD patterns of the both samples are mainly composed of the constituencies of the kaolinite [JCPDS No. 89–6538] [24]. However, in the case of MK composite, the characteristic peaks of iron oxide [JCPDS No.19–0629] dominated as indicated by the sharper peaks noticed at 2θ values of 30°, 35.3°, 43°, 53.3°, 56.8°, and 62.5° corresponding to the (220), (311), (400), (422), (511), and (440) planes, respectively [25]. The sharper peaks observed in the XRD pattern of MK composite are also an indication of higher iron oxide content within the composite. The XRD patterns were used to estimate the average particle size of the MK composite using Scherrer's equation given by Eq. 4 [26].

$$d = \frac{k\lambda}{\beta cos\theta} \tag{4}$$

Here, the terms k and β represent the Scherrer constant and the wavelength of Cu Ka X-ray (1.5406 Å) and the full width at half-maximum (FWHM) of the XRD peaks and the Bragg diffraction angle, respectively. Using this equation, the average particle size of the MK adsorbent was estimated to be around 17.36 nm.

#### FTIR Analysis

The FTIR spectra obtained for kaolinite and the magnetic iron oxide/kaolinite composite are shown in Fig. 2. For kaolinite, the broad band observed at 3695 cm$^{-1}$ represents the contribution of the hydroxyl groups present on the edge on the kaolinite platelets.The peak observed around 3618 cm$^{-1}$ represents the -OH stretching within the kaolinite sheets [27]. The O-Si–O stretching and deformation and Al-O–H deformation vibration were represented by the

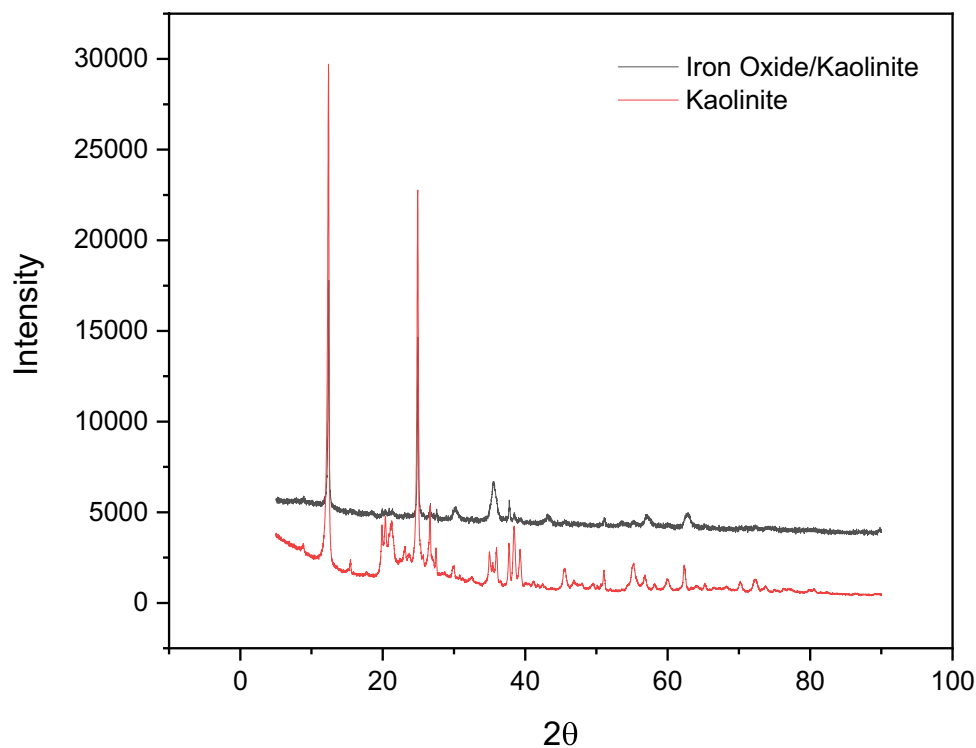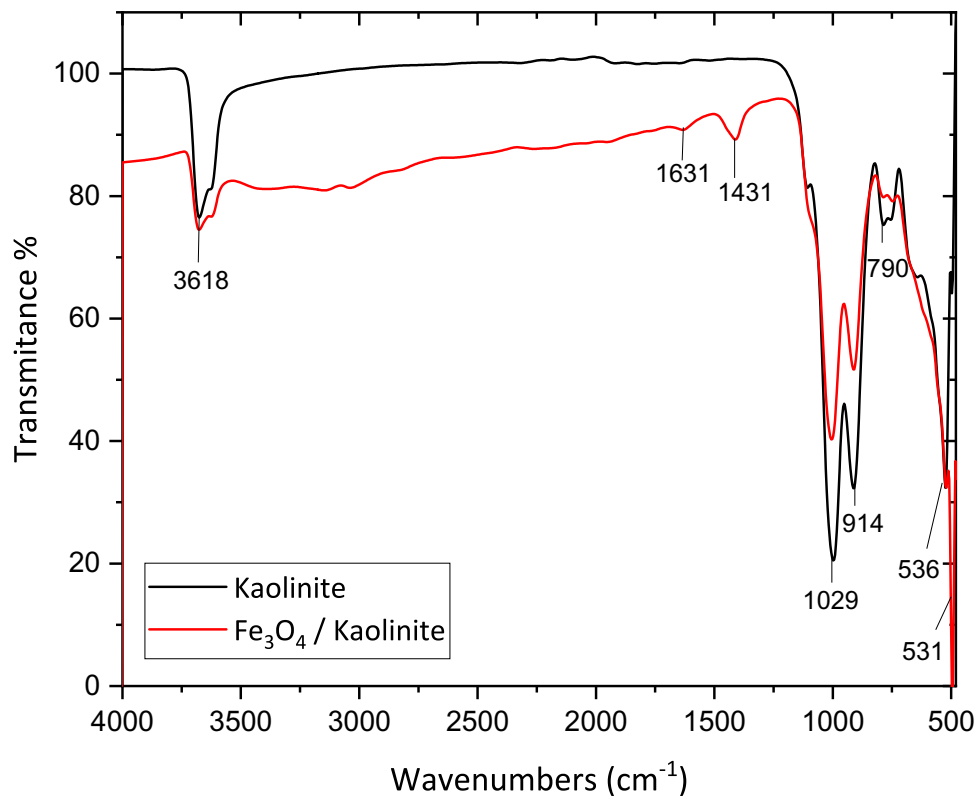**Fig. 1** The XRD patterns of the kaolinite and magnetic iron oxide/kaolinite composite



**Fig. 2** The FTIR spectra of the kaolinite and magnetic iron oxide/kaolinite composite



peaks observed at 1029 and 914 cm$^{-1}$, respectively [28]. The small peak observed at 790 cm$^{-1}$ affirmed the presence of amorphous silica, while the peak observed at 536 cm$^{-1}$ represents the Si–O–Al bond [29]. As for the magnetic iron oxide/kaolinite composite, three additional peaks were observed along with all the peaks observed for kaolinite. The

peak observed at 1631 cm$^{-1}$ for MK composite represents the vibration due to absorbed water. The peak observed at 1431 cm$^{-1}$ represents the C-O–H stretching mode primarily originating ammonia used during the synthesis. Finally, the peak observed at 531 cm$^{-1}$ indicates the presence of Fe–O bonds within the composite [30].

### SEM/EDX Analysis

The SEM images for magnetic iron oxide/kaolinite composite are presented in Fig. 3a. It was observed that the composite contained layers of non-uniform kaolinite halloysites. These halloysites contained small clusters of iron oxide that partly covered its outer surface (highlighted in Fig. 3). The clusters primarily resulted from the aggregation of the nano-sized iron oxide particles whose diameter was calculated according to the Scherrer equation to be around 17.36 nm. This observation further justifies the XRD patterns for the MK composites, where upon formation of the composite the peaks representing the iron oxide patterns became more dominant. An analysis of EDX data (Fig. 3b) obtained for the as-prepared magnetic iron oxide/kaolinite composite showed that the composite primarily contained four major elements, namely iron (Fe), aluminum (Al), silicon (Si), and oxygen (O) [31]. Of the four elements present within the composite, the iron (31.2%) and oxygen (47.0%) were found to be dominant compared to the aluminum (11.2%) and silicon (10.5%). The high content of Fe and O signifies the presence of iron oxide within the composite along with the confirmation of its successful grafting onto kaolinite clay mineral [32].

### Thermogravimetric Analysis

The thermal stability of the kaolinite and magnetic iron oxide/kaolinite composite was analyzed over a temperature range of 30 to 900 °C and the obtained TGA curves are presented in Fig. 4 below. The kaolinite exhibited almost no weight loss (around 0.5%) up to 450 °C. However, between 450 and 700 °C, an overall weight loss of 12% was observed. Note that kaolinite is hydrous silicate minerals of clay that structurally consists of Si–O tetrahedral sheet and Al-O(OH) octahedral sheets. They noticed that at high temperature, the structural water present within these minerals is driven off converting the kaolinite to metakaolinite. Therefore, the observed 12% weight loss can be attributed to the loss of structural water. In case of magnetic kaolinite composite, a steep weight loss of 4% was observed up to a temperature of 250 °C, due to the loss of residual physisorbed water and other organic solvents. A further loss of 1% was observed at a temperature of 450 °C due to loss of chemisorbed water and other organic solvents. Beyond the temperature of 450 °C, a gradual loss of 6% was observed due to the removal of structural water from the kaolinite present within the MK composite.
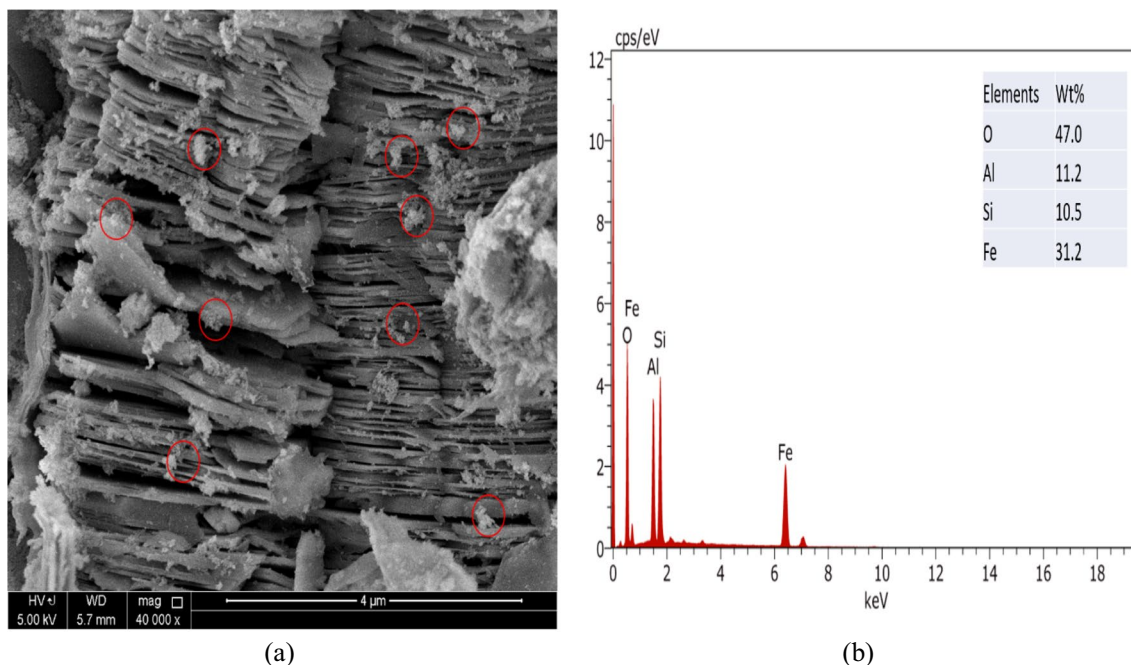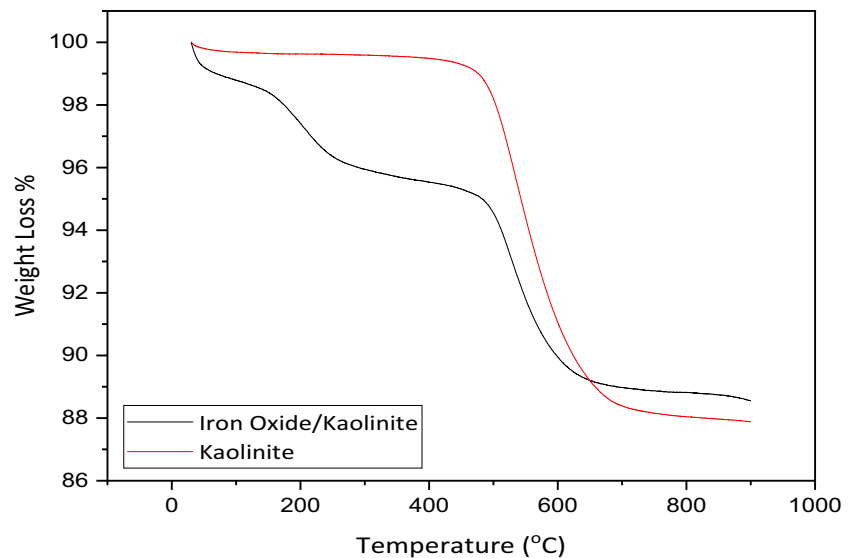


(a)    (b)

**Fig. 3** **A** SEM and **b** EDX of as-prepared magnetic iron oxide/kaolinite composite

**Fig. 4** The TGA curves of the kaolinite and magnetic iron oxide/kaolinite composite



## XPS Analysis

The XPS analysis was carried out to perform a surface chemical analysis of the magnetic iron oxide-kaolinite composite. The survey spectrum obtained (Fig. 5a) shows the presence of Fe 2p, O 1 s, Si 2p, and Al 2p peaks which verifies the presence Fe, O, Si, and Al elements within the MK composites. On analyzing the Fe 2p XPS spectrum (Fig. 5b), two broad peaks associated with the Fe $2p_{3/2}$ (710.5 eV) and Fe $2p_{1/2}$ (723.7 eV) were observed. These peaks affirm of the presence of iron oxide within the MK composite [33]. Further analyzing the two peaks, it was observed that they can be deconvoluted into three separate Fe 2p core level peaks, one suggesting the presence of the $Fe^{2+}$ (Fe $2p_{3/2}$: 709.5 eV, Fe $2p_{1/2}$: 722.7 eV and a satellite: 717.2 eV) and the other of that of the $Fe^{3+}$ ions (Fe $2p_{3/2}$: 711.5 eV, Fe $2p_{1/2}$: 724.7 eV and a satellite: 732.3 eV) [34]. Based on this, it can be suggested that Fe ions are present in mixed valence state in the MK composite. Deconvolution of the Si 2p XPS spectrum (Fig. 5c) resulted in three separate peaks. The small peak observed at the binding energy of 99.3 eV shows the presence of some pure silicon on the surface of the composite. While the relatively broad peaks observed at binding energies of 101.1 eV and 101.7 eV indicate the presence of $Si^{2+}$ ions and $SiO_2$, respectively [35]. Following the same procedure, the XPS spectrum of the Al 2p (Fig. 5d) could also be divided into two peaks that showed the presence of metal aluminum (72.7 eV) and $Al_2O_3$ species (74.8 eV) on the surface of as-prepared composite [36]. Finally, in the deconvolution of the O 1 s XPS spectrum (Fig. 5e), four distinct peaks were generated. The broad peak obtained at 530.0 eV shows the presence of Fe–O species associated with iron oxide [37]. The peak 528.7 eV could be resulted from the interactions of Fe–O species with the other two

metals (Al, Si) within the composite. The two other peaks observed at 531.74 eV and 532.15 eV attribute to the presence of native oxygen and residual oxygen containing groups like the hydroxyl groups within the composite [36, 37].

## VSM Analysis

The magnetic properties of the as-prepared magnetic iron oxide/kaolinite composite were tested and the obtained results are presented in Fig. 6a below. It can be observed that the MK composite generated a very narrow hysteresis loop. The saturation magnetism was around 94.43 emu/g, which is indicative of the superparamagnetic behavior of the as-prepared MK composite. Furthermore, it also reaffirms the EDX results, where the MK composite was found to have very high content of iron oxide. It is due to this magnetic property; the as-prepared MK composite could be easily removed from any adsorption process in the presence of an external magnetic field as shown in Fig. 6b.

## Effect of pH

The effect of pH on the adsorption of Congo red dye was investigated by performing batch adsorption experiments at different pH. Experiments were conducted using an adsorbent dose of 1.0 g.L$^{-1}$, while shaker speed was maintained at 200 rpm and fixed Congo red dye concentration of 20 mg.L$^{-1}$. The temperature was maintained at 303 K and obtained results are presented in Fig. 7a. It is to be noted that several studies have indicated that the color of the Congo red dye changes to dark blue at lower pH values [38]; therefore, to study the effect of pH while the color of the dye was still intact, a pH range of 5–11 was chosen. It is evident from Fig. 7a that the absorption
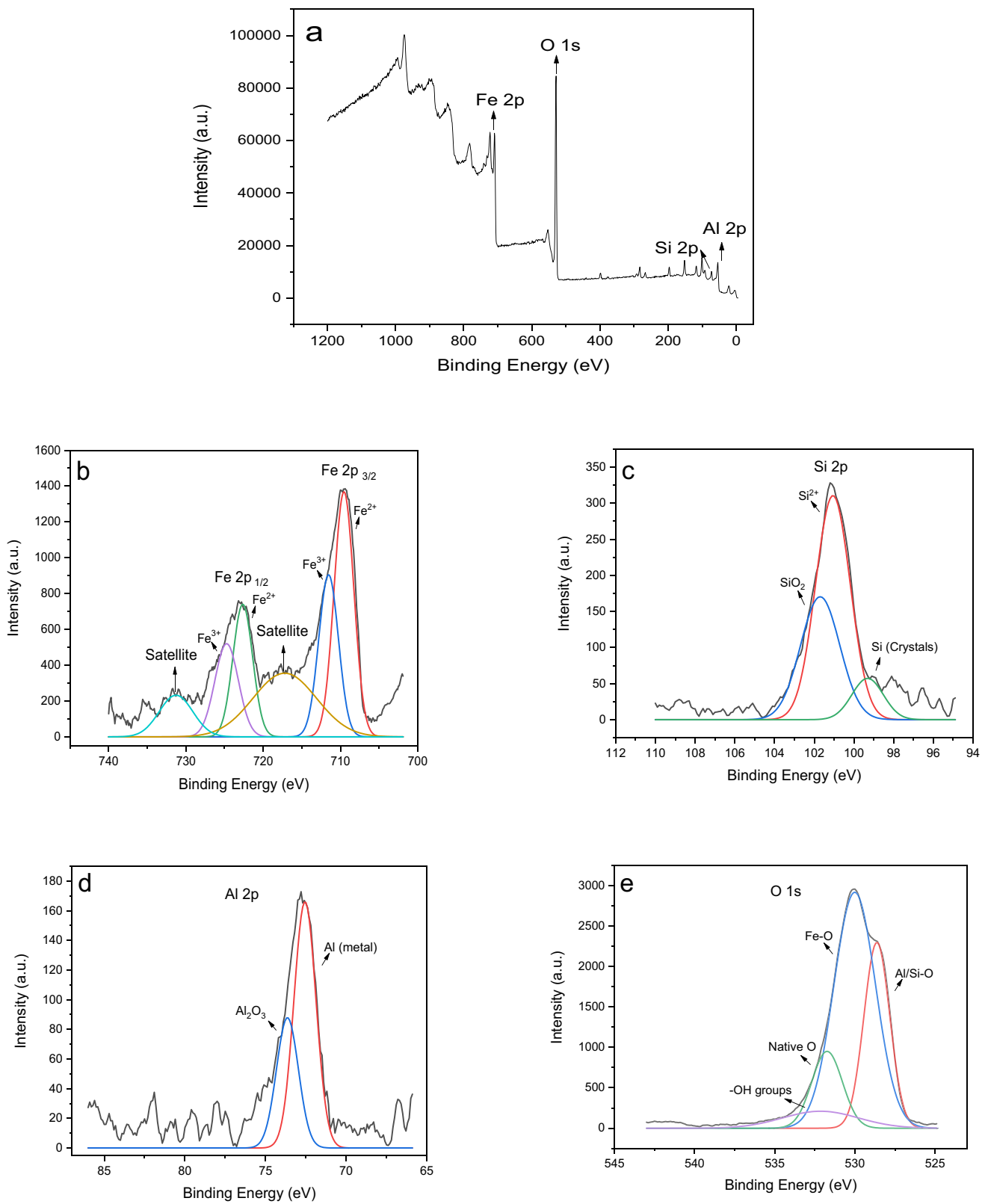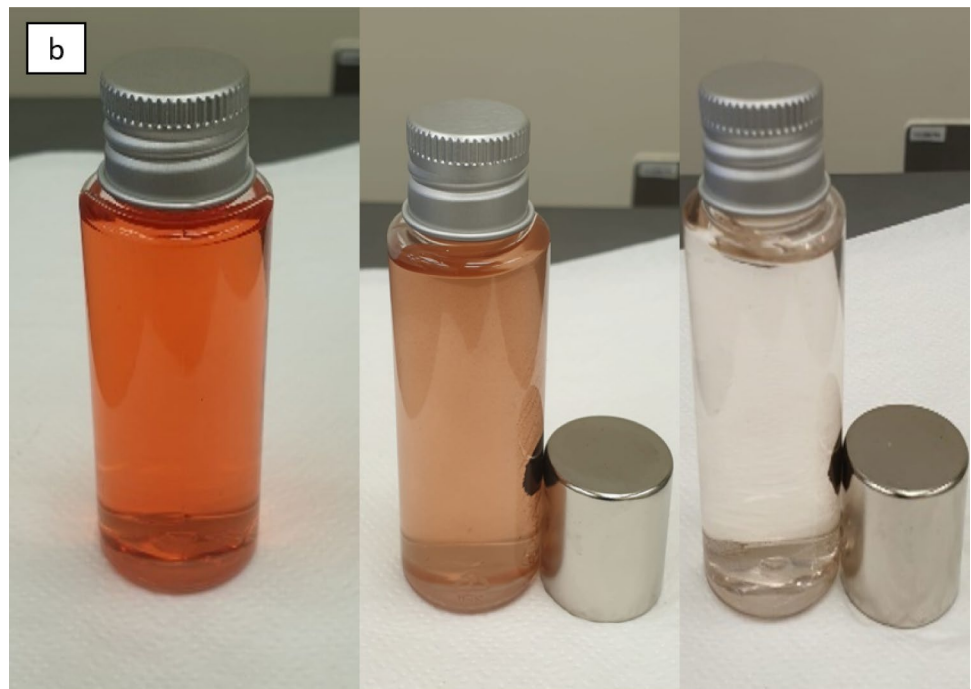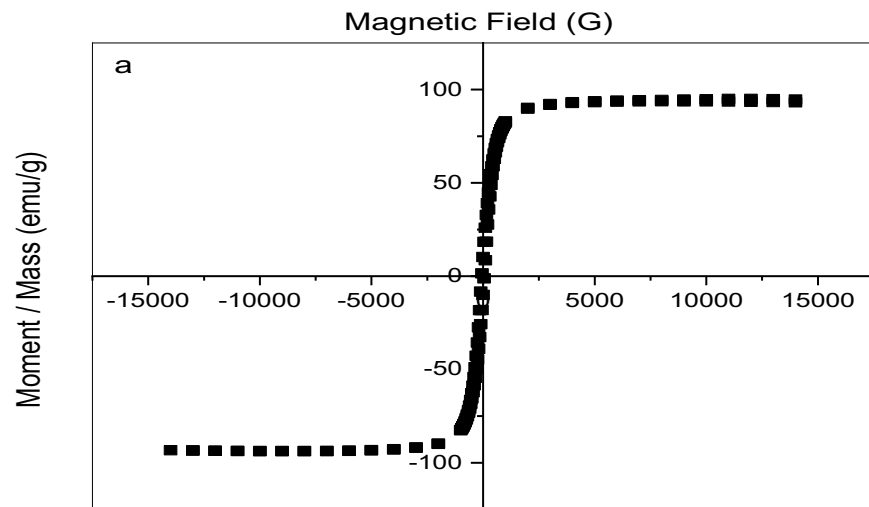
**Fig. 5** XPS spectra of magnetic iron oxide-kaolinite composite: survey (**a**), Fe 2p (**b**), Si 2p (**c**), Al 2p (**d**), and O 1 s (**e**) XPS spectrums

**Fig. 6** The VSM curve obtained for the magnetic iron oxide-kaolinite composite (**a**) magnetic separation of MK composite after adsorption of Congo red dye (**b**)





performance improved as pH value approached towards neutral medium. It increased from a value of 96% at pH of 5.5 to almost 99% at 7.7. However, beyond that pH value, a gradual dip was noticed in the absorption performance of the Congo red dye and went down to almost 75% at pH 11. Since the natural pH of the Congo red dye solution was in the range of 5.5 to 5.8 and only small improvement could be achieved by varying the pH to 7.7, the adsorption studies were conducted at the natural pH condition of the Congo red dye solution.

## Effect of Adsorbent Dosage

The effect of MK dosage ranging from 0.2 to 2 g.L$^{-1}$ on the removal 20 mg.L$^{-1}$ of Congo red dye was investigated at 303 K; a shaker speed of 200 rpm and at natural pH is shown in Fig. 7b. The amount of Congo red dye removed increased with the increase in MK dosage. This behavior can be attributed to the fact that with the increase in the adsorbent dosage, more adsorption sites became accessible, which in turn increased the adsorption surface area favoring adsorption of
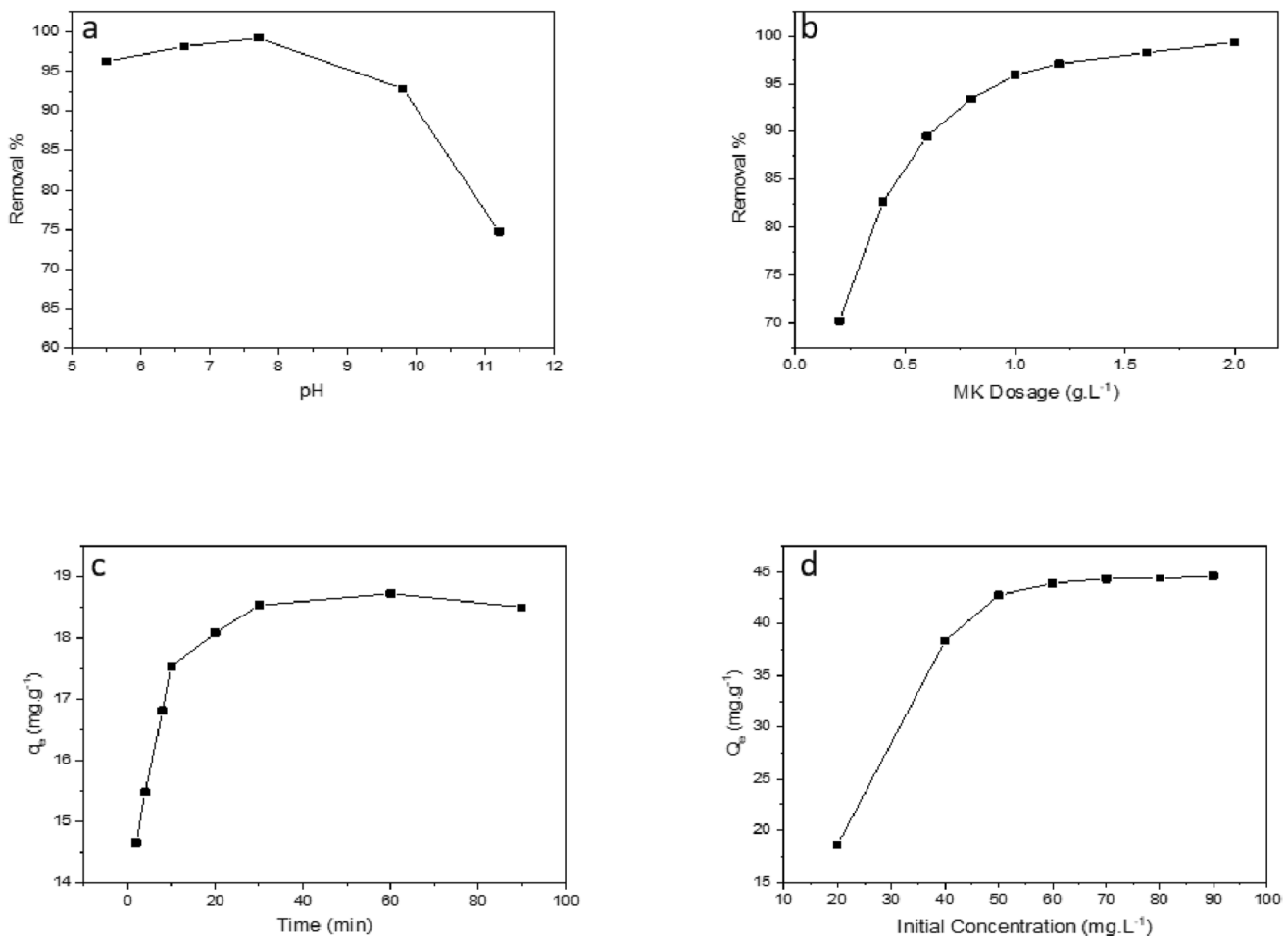
**Fig. 7** The effect of pH (**a**), dosage (**b**), contact time (**c**), and initial concentration (**d**) on Congo red adsorption using the MK composite

more Congo red dye. With the initial dose 0.2 g.L$^{-1}$, 70% of the Congo red dye was removed in 60 min. A gradual increase in Congo red adsorption (82 to 93%) was observed between the MK dosage of 0.4 to 0.8 g.L$^{-1}$. A maximum removal efficiency of 96% was obtained at adsorbent dosage of 1.0 g.L$^{-1}$; hence, it was chosen as the optimum dosage for the Congo red adsorption experiments.

## Effect of Contact Time

The effect of contact time on Congo red dye adsorption was assessed by determining the amount of Congo red adsorbed at different time intervals. An adsorbent dosage of 1.0 g.L$^{-1}$, initial dye concentration of 20 mg.L$^{-1}$, natural pH, shaker speed of 200 RPM, and a temperature of 303 K were used to perform this study and the obtained results are presented in Fig. 7c below. It is evident from Fig. 7c that within the first 2 min, around 15.5 mg.L$^{-1}$ of the dye was adsorbed by the MK adsorbent. The adsorption reached around 18 mg.L$^{-1}$ after 10 min; beyond this, the adsorption process slowed

down until it reached equilibrium at 18.51 mg.L$^{-1}$ at 30 min. No further adsorption was observed beyond this time.

## Effect of Initial Congo Red Concentration

The effect of Congo red dye concentration on the adsorption performance was studied by varying the initial concentrations of the dye under the same experimental conditions (adsorbent dose 1.0 g.L$^{-1}$, natural pH, time 120 min, shaker speed of 200 rpm, and temperature 323 K) as shown in Fig. 7d. It was observed that the adsorption performance is dependent on the initial dye concentration. Firstly, the maximum adsorption capacity improved from 18.51 mg.g$^{-1}$ at the initial Congo red concentration 20 mg.L$^{-1}$ to 42.76 mg.g$^{-1}$ at 50 mg.L$^{-1}$. This resulted from the availability of more dye molecules to be absorbed on the surface of the MK adsorbent. However, starting from initial dye concentration of 60 mg.L$^{-1}$ and beyond, the adsorption capacity became constant at around 45 mg.g$^{-1}$. This phenomenon resulted from the decrease in the availability of the competitive adsorbent

sites with the increase in the initial dye concentration rendering it more stable at higher concentrations. Similarly, the effect of contact time on the Congo red adsorption process was also assessed at 20 mg.g$^{-1}$ at different time intervals at an adsorbent dose of 0.1 g.L$^{-1}$, natural pH, and temperature of 303 K.

## Adsorption Isotherms

Analysis of the adsorption isotherms is essential to understand the interactions between the surface of MK adsorbent and the Congo red molecules. Typically, the adsorption isotherms or the equilibrium studies reveal the capacity of the adsorbents. Adsorption isotherm equations are characterized by some constants or values that disclose the properties related to the surface of the adsorbent and its affinity towards the adsorbate. Therefore, it is imperative to relate the obtained experimental

equilibrium data to different isotherm equations for proper depiction of the Congo red adsorption using MK adsorbent [39]. Hence, the adsorption data were fitted to three different isotherms: namely, Langmuir, Freundlich, and Temkin by performing non-linear regression using OriginPro. The obtained experimental data along with the fitted isotherms at three different temperatures (303 K, 313 K, and 323 K) are shown in Fig. 8, and the inter-related parameters are presented in Table 1.

### Langmuir Isotherm

The Langmuir isotherm assumes that the maximum adsorption occurs due to the formation of a monolayer by the adsorbate on the surface of the adsorbent. It further assumes that the energy required for adsorption process is constant, and once the adsorbate, i.e., the Congo Red molecule has occupied a site on the surface of the MK adsorbent, no
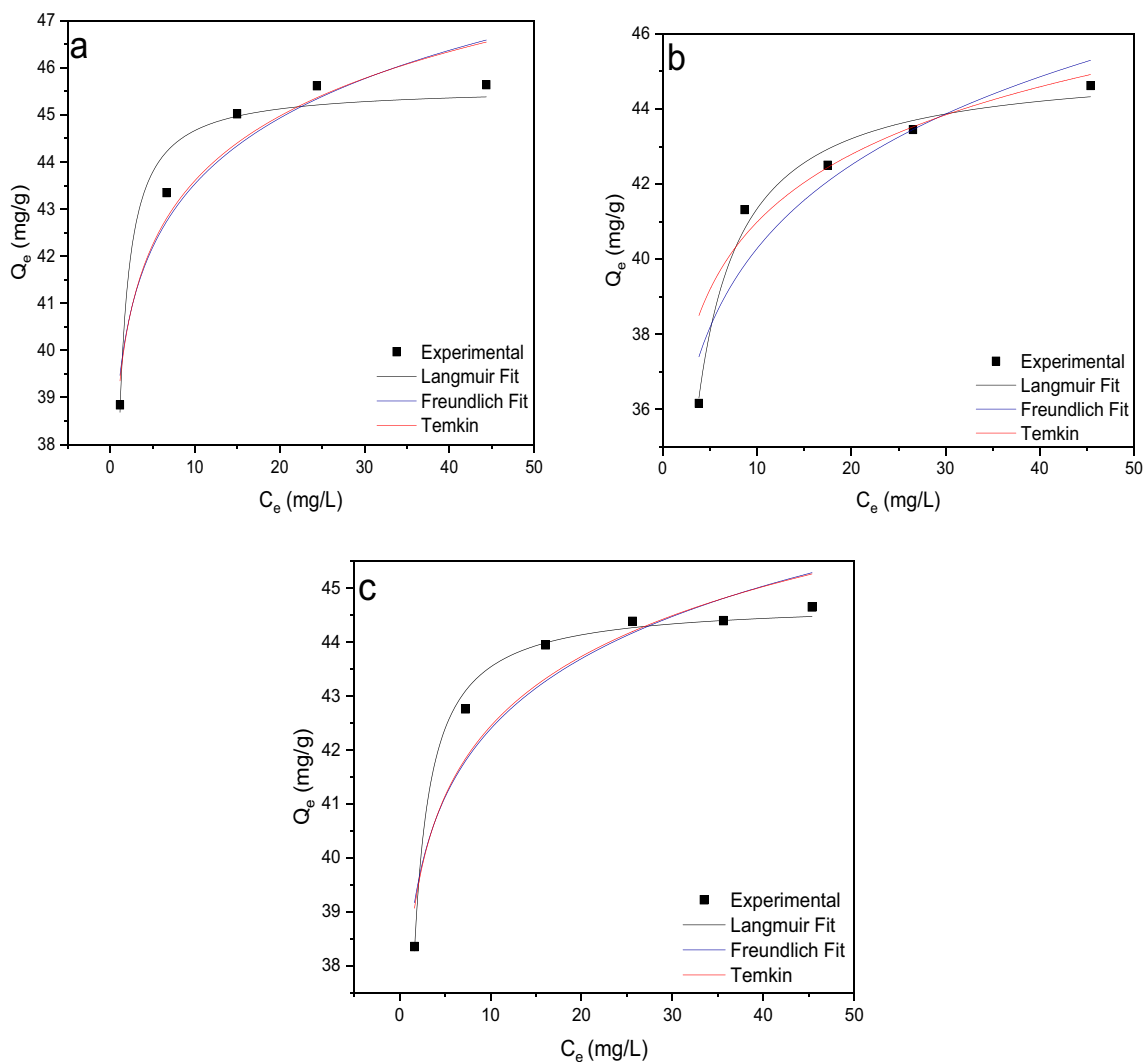


Fig. 8 The observed adsorption isotherms for Congo red adsorption using MK adsorbent at 303 K (**a**), 313 K (**b**), and 323 K (**c**)

**Table 1** Isotherm model parameters for the adsorption of Congo red using MK composite

| Isotherm | Parameters | Temperature (K) | | |
|---|---|---|---|---|
| | | 303 | 313 | 323 |
| Langmuir | $q_m$ (mg.g$^{-1}$) | 45.59 | 44.99 | 44.74 |
| | $K_L$ (L.mg$^{-1}$) | 4.82 | 4.31 | 3.60 |
| | $R^2$ | 0.97 | 0.91 | 0.99 |
| Freundlich | $K_f$ (mg.g$^{-1}$) (L.mg$^{-1}$)$^{1/n}$ | 33.70 | 38.80 | 38.33 |
| | $n$ | 12.90 | 19.08 | 22.86 |
| | $R^2$ | 0.90 | 0.90 | 0.90 |
| Temkin | $b$ (KJ/mol) | 1.08 | 1.27 | 2.63 |
| | $\alpha$ (L/g) | $2.30\times10^7$ | $9.92\times10^7$ | $5.86\times10^{17}$ |
| | $R^2$ | 0.94 | 0.91 | 0.91 |

further adsorption will occur on the same site [40]. The non-linear form of the governing equation for Langmuir isotherm model is given by Eq. 5.

$$q_e = \frac{q_m K_L C_e}{1 + q_m K_L C_e} \tag{5}$$

Here, the terms $q_m$ and $K_L$ stands for the maximum amount of Congo red adsorbed by the MK composite and Langmuir constant, respectively. Both terms were determined by nonlinear regression. From Fig. 8a and Table 1, the model could successfully depict the Congo red adsorption process using the MK adsorbent for all three temperatures with a correlation coefficient, $R^2$, of more than 0.90. The maximum adsorption capacity of MK adsorbent at 303 K was 45.59 mg.g$^{-1}$. A further increase in temperature to 313 K resulted in the amount to be slightly reduced to 44.99 mg.g$^{-1}$ and almost the same was observed when the temperature was increased to 323 K (44.74 mg.g$^{-1}$). Based on these results, it can be concluded that the maximum Congo red adsorption capacity of the MK adsorbent remains unaffected with the increase in temperature. To further predict whether an adsorption process is favorable or not, Hall et al. [41] has proposed a dimensionless separation factor or equilibrium parameter, "$R_L$," based on the obtained Langmuir constant, "$K_L$," and it is given Eq. 6.

$$R_L = \frac{1}{1 + K_L C_e} \tag{6}$$

The adsorption process is considered to be favorable when the $R_L$ value falls between zero and unity and it is unfavorable when it is greater than unity. Moreover, the adsorption is linear when $R_L$ equals unity and irreversible when it equals zero. The calculated values of $R_L$ were for Congo red adsorption using MK adsorbent was observed to be within the range 0.052 to 0.58, which indicates the adsorption process was favorable.

**Freundlich Isotherm**

The Freundlich isotherm model is an empirical model which assumes that adsorption occurs on heterogeneous surface or at multiple adsorption sites. According to this model, Congo red molecules will first bind with stronger binding sites of the MK adsorbent and the binding strength of the site will keep decreasing as more Congo red molecules get attached to the site [42]. The non-linear form of the governing equation for Freundlich isotherm is given by Eq. 7.

$$q_e = K_f C_e^{\frac{1}{n}} \tag{7}$$

Here, the terms "$K_f$" represents the relative adsorption capacity of the absorbent; i.e., the higher the value of $K_f$, the higher will be the adsorption capability of the MK adsorbent, while the term "n" denotes the type and intensity of the adsorption. When the value of $n$ equals unity, the adsorption is linear. Moreover, the adsorption process accepted to be chemical in nature when the value of $n$ is below unity, whereas a value greater than unity indicates that the adsorption process is favorable and physical in nature [43]. From Fig. 8b and Table 1, it is observed that the Freundlich isotherm could also depict the Congo red adsorption process using the MK adsorbent for all three temperatures with the correlation coefficient, $R^2$, of 0.90 (in all cases). The $K_f$ value or the relative adsorption capacity of the MK adsorbent was found to be 33.70 (mg.g$^{-1}$) (L.mg$^{-1}$)$^{1/n}$ for 303 K. However, with the increase in temperature to 313 K, the Congo red adsorption capability to for the MK adsorbent also increased to 38.80 (mg.g$^{-1}$) (L.mg$^{-1}$)$^{1/n}$. Further increase in temperature resulted in a slight decrease in the adsorption capability. Moreover, an evaluation of the obtained values for $n$ shows that it was greater than unity for all three different temperatures, indicating a physical adsorption process. It also indicates that the adsorption is favorable agreeing with the findings of the Langmuir isotherm.

**Temkin Isotherm**

The Temkin isotherm assumes that the free energy of adsorption is essentially a function of the surface coverage. The model contains factors that takes into account the interactions between the Congo red molecules and MK adsorbate [44]. The Temkin isotherm model is denoted by the following non-linear Eq. 8:

$$q_e = \beta \ln \alpha C_e \tag{8}$$

Here, $\alpha$ is an equilibrium binding constant and $\beta$ represents the heat of adsorption which is determined by Eq. 9.

$$\beta = \frac{RT}{b} \tag{9}$$

where $R$ is the universal gas constant, $T$ is the temperature, and $b$ represents the variation of the adsorption energy. From Fig. 8c and Table 1, it is evident that the Temkin isotherm could also be fitted with the obtained experimental data with correlation coefficient exceeding 0.94 at all three temperatures. The binding energy of Congo red adsorption using MK adsorbent showed a gradual increase with the increase in temperature (Table 1). It was observed to around 1.08 kJ.mol$^{-1}$, 1.27 kJ.mol$^{-1}$, and 2.63 kJ.mol$^{-1}$ at 303 K, 313 K, and 323 K, respectively. Since at all three temperatures, the binding energy was less than 8 kJ.mol$^{-1}$, it can be suggested that the adsorption process proceeds physisorption [45]. This finding agrees with the previous findings of the Langmuir and Freundlich isotherms. Therefore, based on the results, it can be concluded that the Congo red dye is adsorbed on the MK adsorbent via physical adsorption. All three isotherms could be used to interpret the observed experimental data. However, based on Fig. 8 and correlation coefficient, it can be suggested that the Langmuir isotherm model better fits the Congo red adsorption using MK adsorbent followed by the Temkin and Freundlich isotherm models.

## Adsorption Kinetics

Analysis of the adsorption kinetics is important to illustrate the effect of the contact time on the Congo red adsorption using MK adsorbent. Different adsorption kinetics models are applied to perform the adsorption kinetics studies. The adsorption kinetics models help in quantifying the adsorption rates along with providing essential insights on the mechanism of the Congo adsorption using MK adsorbent [2]. Three different adsorption kinetics models, namely, pseudo-first-order, pseudo-second-order, and intraparticle diffusion model were used to evaluate the obtained experimental data on adsorption kinetics. The obtained adsorption kinetics data at three different temperatures (303 K, 313 K, and 323 K) fitted in three different kinetics models are shown in Fig. 9 and the inter-related parameters are presented in Table 2.

### Pseudo-First-Order Kinetics

The pseudo-first-order kinetics also known as the Lagergren first order is one of the most commonly used models to analyze kinetics of the adsorption processes [46]. The model suggests that the rate of Congo red dye adsorption is directly proportional to the number of the free sites available on the surface of the MK adsorbent. The linear form of the pseudo-first-order kinetics is given by Eq. 10 [47].

$$\ln\left(q_e - q_t\right) = \ln q_e - k_1 t \qquad (10)$$

Here, the terms $q_e$ and $q_t$ (mg/g) represent the amount of Congo red adsorption using MK adsorbent at equilibrium and time $t$ (min), respectively, while $k_1$ (min$^{-1}$) is the constant for pseudo-first-order kinetics. A plot of $\ln(q_e\text{-}q_t)$ against the time $t$ as shown in Fig. 3a was used to obtain all required parameters to interpret the Congo adsorption kinetics data based on Lagergren model and they are summarized in Table 2. It was observed that the $q_e$ obtained from the plots were much lower than actual experiment $q_e$ recorded during the experiment for all three temperatures. Moreover, the correlation co-efficient of this model was also low ($R^2 = 0.77$–0.84). Based on these results, it can be suggested that the Congo red adsorption kinetics do not obey the pseudo-first-order model.

### Pseudo-Second-Order Kinetics

Pseudo-second-order model is another popular kinetics model employed to interpret the adsorption kinetics data [48]. This model takes into account the adsorption capacity of the MK adsorbent based on the concentration of the Congo red solution [49]. The linear form of the pseudo-second-order kinetics is given by Eq. 11.

$$\frac{t}{q_t} = \frac{1}{k_2^2 q_e} + \frac{t}{q_e} \qquad (11)$$

Here, the term $k_2$ (g.mg$^{-1}$.min$^{-1}$) is the second-order rate constant of the adsorption process. A plot of $t/q_t$ against the time $t$ as shown in Fig. 3b was used to obtain all required parameters to interpret the Congo adsorption kinetics data based on the pseudo second order kinetics model and they are summarized in Table 2. From Fig. 3b and Table 2, it is evident that the kinetics data obtained could be successfully fitted to this model with the correlation coefficient, $R^2$, close to unity for all three different temperatures (303 K, 313 K, and 323 K). The $k_2$ values of the Congo red adsorption decreased slightly with the increase in temperature from 303 to 313 K (0.086 to 0.080). However, it remained relatively stable as the observed $k_2$ values over all three temperatures were not significantly different. It can be concluded that the adsorption kinetics of the Congo red dye remains relatively unaffected with the increase in temperature. Moreover, from Table 2, it is also evident that the generated adsorption amount at equilibrium is very close to the experimentally observed amount. These results are suggestive of the fact that the pseudo-second-order kinetic model is suitable in describing the Congo red adsorption using MK adsorbent than the pseudo-first-order model.

### Adsorption Mechanism

The obtained experimental kinetics data were further analyzed using the intraparticle diffusion model to further
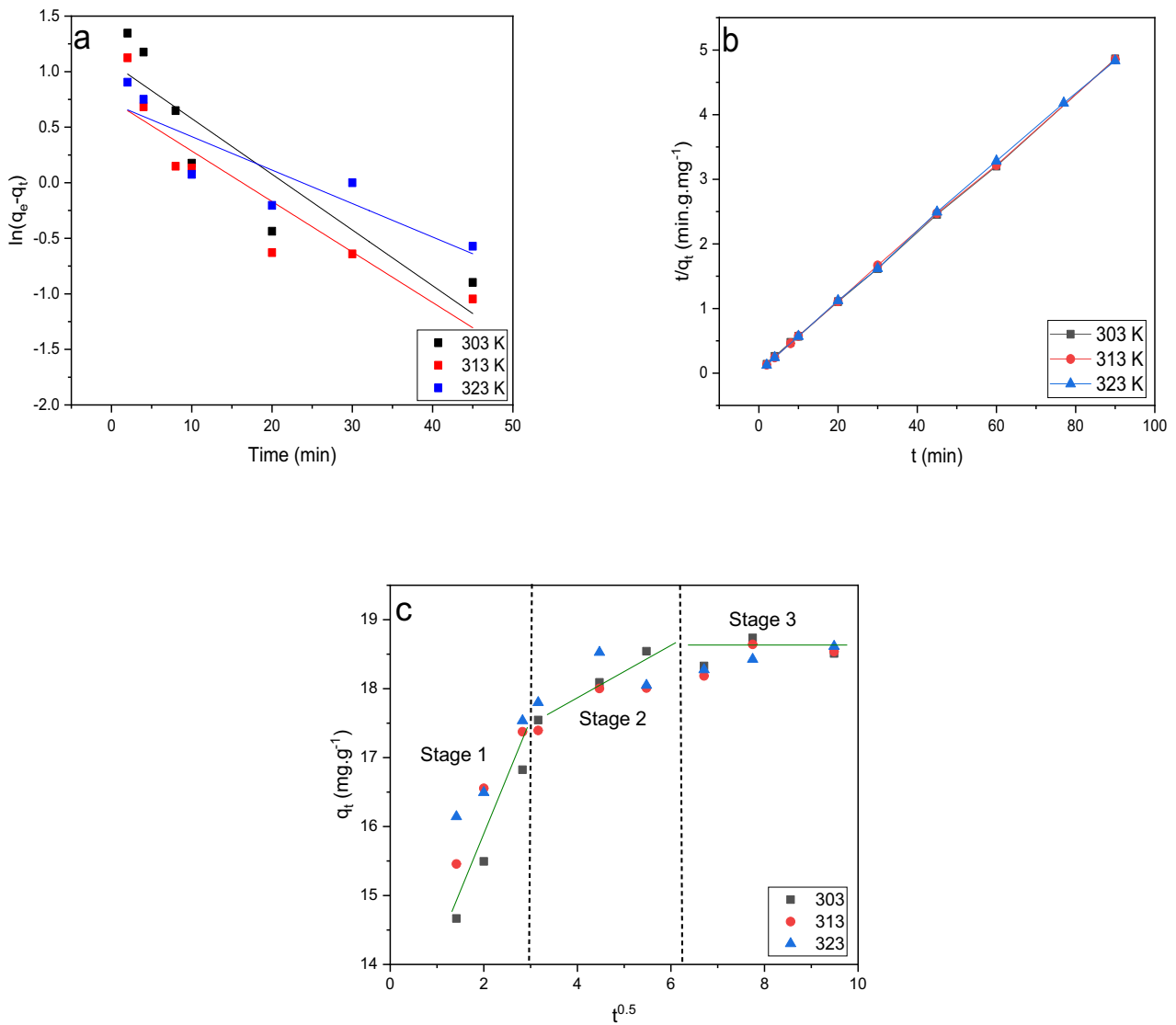
**Fig. 9** Pseudo-first-order (**a**), pseudo-second order (**b**), and intraparticle diffusion models (**c**) at different temperatures for Congo red adsorption using MK adsorbent

**Table 2** Kinetics parameters for the adsorption of Congo red using MK composite

| Kinetic model | Parameters | Temperature (K) | | |
|---|---|---|---|---|
| | | 303 | 313 | 323 |
| Pseudo-first order | $q_{c,calculated}$ (mg.g$^{-1}$) | 4.44 | 2.10 | 2.00 |
| | $q_{e,experimental}$ (mg.g$^{-1}$) | 18.51 | 18.54 | 18.61 |
| | $k_1$ (L.min$^{-1}$) | 0.104 | 0.046 | 0.031 |
| | $R^2$ | 0.77 | 0.84 | 0.79 |
| Pseudo-second order | $q_{c,calculated}$ (mg.g$^{-1}$) | 18.6 | 18.65 | 18.72 |
| | $q_{e,experimental}$ (mg.g$^{-1}$) | 18.51 | 18.54 | 18.61 |
| | $k_2$ (g.mg$^{-1}$.min$^{-1}$) | 0.086 | 0.080 | 0.081 |
| | $R^2$ | 0.99 | 0.99 | 0.99 |

**Table 3** Intraparticle diffusion model parameters and correlation coefficients for CR adsorption using MK adsorbent at different temperatures

| Temperature (K) | Stage | $k_{di}$ (g.mg$^{-1}$.min$^{-0.5}$) | $C_i$ | $R^2$ |
|---|---|---|---|---|
| 303 | 1 | 1.53 | 12.48 | 0.99 |
| | 2 | 0.92 | 11.65 | 0.96 |
| | 3 | 0.78 | 9.48 | 0.99 |
| 313 | 1 | 1.33 | 13.69 | 0.97 |
| | 2 | 0.85 | 11.74 | 0.98 |
| | 3 | 0.67 | 11.13 | 0.95 |
| 323 | 1 | 0.81 | 14.95 | 0.99 |
| | 2 | 0.63 | 13.22 | 0.95 |
| | 3 | 0.34 | 13.49 | 0.99 |

**Fig. 10** Adsorption mechanism of Congo red on MK composites
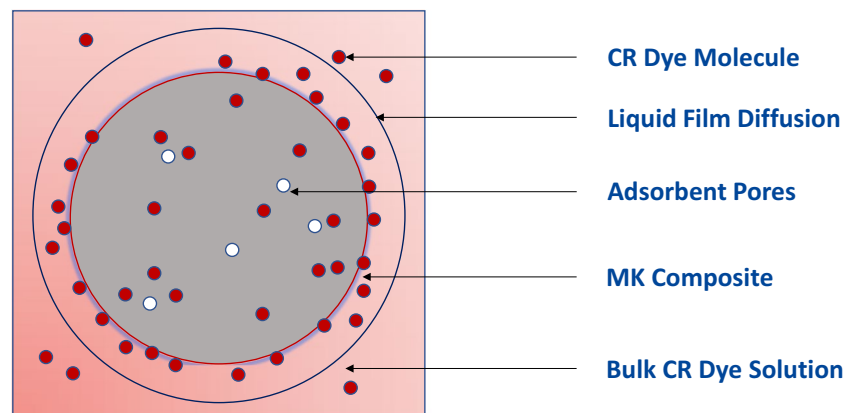


elucidate the mechanism involved in Congo red adsorption using MK adsorbent proposed by Weber and Morris [50]. The governing equation for the intraparticle diffusion model is given by Eq. 12.

$$q_t = k_{di} t^{0.5} + C_i \tag{12}$$

Here, the terms $k_{di}$ (mg.g$^{-1}$. min$^{-0.5}$) and $C_i$ represent the rate constant and intercept of stage I of the Congo red adsorption process, respectively. The term $C_i$ provides insights on the thickness of the boundary layer. The higher the value of $C_i$, the thicker will be the boundary. To obtain the required parameters, the amount of Congo red adsorbed by MK adsorbent at a certain time, t ($q_t$), was plotted against the square root of the time at different temperatures (303 K, 313 K, and 323 K). The obtained plot for at all three temperatures is presented in Fig. 3c. It was observed that the plot did not exhibit any linear relationship over the entire experimental time at any temperature. However, upon further analyzing the plot, it was observed that it can be separated into three separate regions indicating that the adsorption process was happening in three stages. Such adsorption process with multi-linear stages were first explained by Lorenc-Grabowska and Gryglewicz [39] and their analogy could be employed to interpret the Congo red adsorption process using MK adsorbents. At stage 1, the adsorption occurs due to external surface adsorption. In this stage, the Congo red dye molecules diffuse through the solution to the external surface of the MK adsorbent. At this stage, the adsorption is typically high, and the case is evident from the rate constant, $k_{d1}$, summarized in Table 3 for all three temperatures for Congo red adsorption. In the next stage (stage 2), the Congo red molecules are gradually adsorbed by MK adsorbents. During this stage, the intraparticle diffusion is the rate controlling step. From Table 3, it can be observed that the rate constant in this step is lower than that of the first stage at all three temperatures. In the third or final stage, a significantly lower rate constant was observed. This is due to the fact that by stage 3, most of the Congo red molecules are already adsorbed by the MK adsorbent [51]. In other words, the MK adsorbent has

already attained its maximum adsorption capacity by stage 2; therefore, the intra-particle diffusion begins to level out in the final stages. Previously, SEM analysis confirmed the presence of kaolinite halloysites with $Fe_3O_4$ clusters. It is believed that the Congo red molecules are adsorbed between halloysites and clusters. Based on these observations, it can be suggested that the adsorption mechanism of the Congo red on MK adsorbent could be successfully interpreted via the intra-particle diffusion model. A graphical illustration of the adsorption mechanism is shown in Fig. 10.

## Adsorption Thermodynamics

To further comprehend the effect of temperature on the adsorption of Congo red dyes on the iron oxide-kaolinite composites, various thermodynamic parameters were studied. For this purpose, experiments were conducted on 20 mg/L of Congo red dyes in 50-mL conical flasks at an adsorbent dose of 1 g/L for 90 min at four different temperatures (298 K, 303 K, 313 K, and 323 K). The standard Gibbs free energy was calculated using Eq. 13.
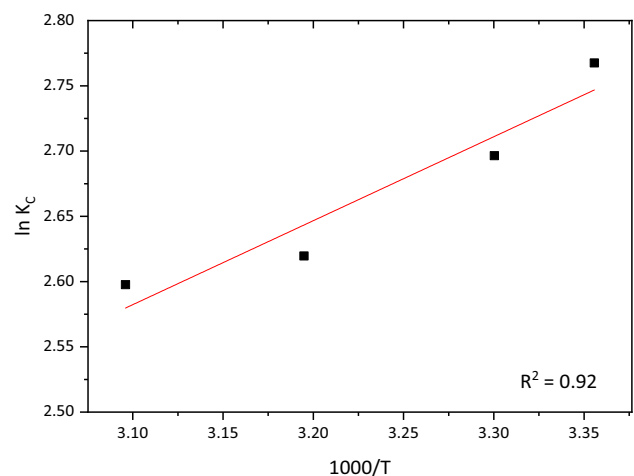


**Fig. 11** Effect of temperature on adsorption of Congo red on iron oxide kaolinite composite

$$\Delta G^O = -RT \, lnK_C \qquad (13)$$

where $K_c$ is the adsorption equilibrium constant. It is defined as the ratio between the amount of dye adsorbed per gram of the MK adsorbent and the concentration of the Congo red dye solution at equilibrium, while the terms $R$ and $T$ stand for the universal gas constant (8.314 $J.mol^{-1}.K^{-1}$) and the temperature, respectively. The relation between the Gibbs free energy with enthalpy and entropy is well known and it is given by Eq. 14.

$$\Delta G^0 = \Delta H^0 - T\Delta S^0 \qquad (14)$$

Combining Eq. 13 with Eq. 14, we obtain a relationship between the adsorption equilibrium constant, the enthalpy, and the entropy by the following equation.

**Table 4** Comparison of maximum adsorption capacity $q_m$ and second-order rate constant $k_2$ for adsorption of on MK composite with other adsorbents

| Adsorbent | Conditions | Second order rate Constant, $k_2$ ($g.mg^{-1}.min^{-1}$) | Maximum Adsorption Capacity, $q_m$ ($mg.g^{-1}$) | Ref |
|---|---|---|---|---|
| $Fe_3O_4$@$SiO_2$@Zn-TDPAT | T = 298 K<br>pH = n/a<br>rpm = n/a<br>time = 120 min | $7.44 \times 10^{-3}$ | 17.73 | [56] |
| Kaolinite | T = 303 K<br>pH = n/a<br>rpm = 150<br>time = 24 h | $3.00 \times 10^{-2}$ | 5.44 | [11] |
| $MnFe_2O_4$ | T = 298 K<br>pH = n/a<br>rpm = 180<br>time = 90 min | $1.60 \times 10^{-1}$ | 25.80 | [57] |
| Magnetic $Fe_3O_4$-Kaolinite composite | T = 298 KT<br>pH = 5.5–5.8<br>rpm = 200<br>time = 90 min | $8.60 \times 10^{-2}$ | 45.59 | This Work |
| Magnetic $Fe_3O_4$@graphene | T = 298 K<br>pH = n/a<br>rpm = 150<br>time = 120 min | $1.31 \times 10^{-2}$ | 33.66 | [58] |
| Hallow Zn-$Fe_2O_4$ nanospheres | T = 298 K<br>pH = 6<br>rpm = n/a<br>time = 2 h | - | 16.10 | [59] |
| $Fe_3O_4$@$SiO_2$ | T = 298 K<br>pH = n/a<br>rpm = n/a<br>time = 120 min | - | 14.76 | [56] |
| Magnetite Intercalated Bentonite | T = Ambient<br>pH = 4<br>rpm = N/A<br>time = 105 min | $2.00 \times 10^{-2}$ | 48.00 | [13] |
| PVP-coated $Fe_3O_4$ | T = Ambient<br>pH = 6<br>rpm = 150<br>time = 90 min | $2.43 \times 10^{-3}$ | 113.63 | [60] |
| Chitosan/iron oxide nanocomposite | T = Ambient<br>pH = 7.52<br>rpm = 60<br>time = 24 h | - | 12.86 | [61] |
| Chitosan/Glycerol/iron oxide nanocomposite | T = Ambient<br>pH = 7.55<br>rpm = 60<br>time = 24 h | - | 10.30 | [61] |

$$lnK_C = -\frac{\Delta H^0}{RT} + \frac{\Delta S^0}{R} \qquad (15)$$

Based on this equation, a linear plot of $lnK_C$ versus the inverse of temperature (Fig. 11) was then used to obtain the enthalpy and entropy of the Congo red adsorption using MK adsorbent. The obtained values of Gibbs free energy at four different temperatures along with the enthalpy and entropy are summarized in Table S1. Upon evaluating the $\Delta G^0$ values at four different temperature, we observe that they are negative at all temperature implying that the adsorption of Congo red on the MK adsorbent is spontaneous [43].Typically, $\Delta G^0$ range from $-80$ to $-400$ kJ.mol$^{-1}$ indicates a chemical adsorption process [52], while [53] it was mentioned that the $\Delta G^0$ range of $-20$ to $0$ kJ.mol$^{-1}$ indicates the adsorption is physical in nature. Since the $\Delta G^0$ values of this work are within the later range, it can be concluded that Congo red dye is adsorbed by MK adsorbent via physical adsorption process. Moreover, $\Delta H^0$ value obtained from this work is positive and is equal to 5.35 kJ.mol$^{-1}$, which means that the adsorption is endothermic in nature. And since the $\Delta H^0$ is less than 25 kJ.mol$^{-1}$, it further confirms that the adsorption process being involved is a physisorption in nature [54]. It is noteworthy that this observation of the physical nature of Congo red adsorption using MK composite is in line with the results obtained using Langmuir and Freundlich isotherms. The positive values of $\Delta S^0$ also indicates increased randomness at the MK adsorbent/Congo red interface during the adsorption of Congo red on MK adsorbent [55]. Overall, based on the obtained results from the isotherms and the thermodynamic studies, it is evident that the Congo red dye adsorption on MK composite occurs through physisorption.

## Comparison

The maximum adsorption capability obtained based on the Langmuir isotherm ($q_m$) and the second-order rate constants ($k_2$) obtained based on pseudo-second-order kinetics of MK composite was compared to other clay and iron oxide-based adsorbents for Congo red adsorption recently reported in the literature and summarized in Table 4. Among all the adsorbents compared, it was observed that the adsorption capacity of the MK composite was significantly higher (eight times) than the raw kaolinite; the same was observed upon comparing their second-order rate constant. Compared to the magnetite intercalated bentonite, another iron oxide-enhanced clay-based adsorbent, the adsorption capacity of the MK composite was found to be slightly lower (48.00 to 45.59 mg.g$^{-1}$). However, the second-order rate constant of the MK composite ($8.60 \times 10^{-2}$ g.mg$^{-1}$.min$^{-1}$) was four times higher than the magnetite intercalated bentonite ($2.00 \times 10^{-2}$ g.mg$^{-1}$.min$^{-1}$). This case of higher adsorption

capacity yet lower rate constant was also true for PVP-coated $Fe_3O_4$. Therefore, based on its relatively high adsorption capacity and high pseudo-second-order rate constant, MK composite can be a promising adsorbent for Congo red removal from aqueous solutions and a potential adsorbent for other organic pollutants that need to be investigated.

## Conclusions

This study showed that the magnetic iron oxide/kaolinite or MK composite is a potential adsorbent for removal of Congo red dyes from aqueous solutions. The MK composite was synthesized via co-precipitation method and characterized using XRD, FTIR, SEM/EDX, TGA, XPS, VSM, and zeta potentials analysis. Congo red adsorption experiments were conducted using the prepared MK composite. Experimental parameters like pH, adsorbent dosage, contact time, and initial dye concentration were found to have a significant effect on the Congo red adsorption process. Adsorption isotherm studies were conducted by fitting the experimental data to Langmuir, Freundlich, and Temkin isotherms. Langmuir isotherm was found to be the most suitable in fitting the experimental data and the maximum adsorption capacity of the MK composite was found to be 45.59 mg.g$^{-1}$. The adsorption kinetics studies were conducted by fitting the experimental kinetics data into pseudo-first-order and pseudo-second-order models. The pseudo-second-order model was found suitable to interpret the adsorption kinetics data. Further analysis of the kinetic data revealed that the adsorption mechanism could be explained via intraparticle diffusion model. Study of the adsorption thermodynamics of Congo red adsorption on MK composite revealed that the adsorption process was spontaneous, endothermic, and physical in nature. Finally, comparison with other clay and iron oxide-based composite adsorbents revealed that the MK adsorbent has relatively high adsorption capacity and high pseudo-second-order rate constant. Hence, the synthesized MK adsorbent exhibits a high potential to be used as an adsorbent for removal of Congo red dye as well as other organic pollutants from wastewater streams.

## Declarations

**Ethical Approval** There was no ethical approval required in this work.

**Competing Interests** The authors declare no competing interests.

## References

1. Dawood S (2012) Sen TK (2012) Removal of anionic dye Congo red from aqueous solution by raw pine and acid-treated pine cone powder as adsorbent: equilibrium, thermodynamic, kinetics, mechanism and process design. Water Res 46(6):1933–1946. https://doi.org/10.1016/j.watres.2012.01.009

2. Lei C, Zhu X, Zhu B, Yu J, Ho W (2016) Hierarchical NiO–SiO2 composite hollow microspheres with enhanced adsorption affinity towards Congo red in water. J Colloid Interface Sci 466:238–246. https://doi.org/10.1016/j.jcis.2015.12.035

3. Lei C, Pi M, Jiang C, Cheng B, Yu J (2016) Synthesis of hierarchical porous zinc oxide (ZnO) microspheres with highly efficient adsorption of Congo red. J Colloid Interface Sci 490:242–251. https://doi.org/10.1016/j.jcis.2016.11.049

4. Shan R-r, Yan L-g, Yang Y-m, Yang K, Yu S-j, Yu H-q, Zhu B-c, Du B (2015) Highly efficient removal of three red dyes by adsorption onto Mg–Al-layered double hydroxide. J Ind Eng Chem 21:561–568. https://doi.org/10.1016/j.jiec.2014.03.019

5. Lim SJ, Kim T-H (2015) Combined treatment of swine wastewater by electron beam irradiation and ion-exchange biological reactor system. Sep Purif Technol 146:42–49. https://doi.org/10.1016/j.seppur.2015.03.021

6. Mahmud N, Benamor A, Nasser MS, Ba-Abbad MM, El-Naas MH, Mohammad AW (2021) Effective heterogeneous Fenton-like degradation of malachite green dye using the core-shell Fe3O4@SiO2 nano-catalyst. ChemistrySelect 6:865. https://doi.org/10.1002/slct.202003937

7. Gaur J, Vikrant K, Kim KH, Kumar S, Pal M, Badru R, Masand S, Momoh J (2023) Photocatalytic degradation of Congo red dye using zinc oxide nanoparticles prepared using Carica papaya leaf extract. Mater Today Commun 22:100339. https://doi.org/10.1016/j.mtsust.2023.100339

8. Sachin, Pramanik BK, Singh N, Zizhou R, Houshyar S, Cole I, Yin H (2023) Fast and Effective Removal of Congo Red by Doped ZnO Nanoparticles. Nanomater 13(3). https://doi.org/10.3390/nano13030566

9. Vinayagam R, Kandati S, Murugesan G, Goveas LC, Baliga A, Pai S, Varadavenkatesan T, Kaviyarasu K, Selvaraj R (2023) Bioinspiration synthesis of hydroxyapatite nanoparticles using eggshells as a calcium source: evaluation of Congo red dye adsorption potential. J Mater Res Technol 22:169–180. https://doi.org/10.1016/j.jmrt.2022.11.093

10. Zhang Q, Qileng A, Li J, Cao Y, Liu W, Liu Y (2023) Grafting a porous metal–organic framework [NH2-MIL-101(Fe)] with AgCl nanoparticles for the efficient removal of Congo red. ACS Omega 8(5):4639–4648. https://doi.org/10.1021/acsomega.2c06300

11. Vimonses V, Lei S, Jin B, Chow CW, Saint C (2009) Kinetic study and equilibrium isotherm analysis of Congo Red adsorption by clay materials. Chem Eng J 148(2–3):354–364. https://doi.org/10.1016/j.cej.2008.09.009

12. Mouni L, Belkhiri L, Bollinger J-C, Bouzaza A, Assadi A, Tirri A, Dahmoune F, Madani K, Remini H (2018) Removal of methylene blue from aqueous solutions by adsorption on kaolin: kinetic and equilibrium studies. Appl Clay Sci 153:38–45. https://doi.org/10.1016/j.clay.2017.11.034

13. Belachew N, Bekele G (2020) Synergy of magnetite intercalated bentonite for enhanced adsorption of Congo red dye. SILICON 12(3):603–612. https://doi.org/10.1007/s12633-019-00152-2

14. Cheng H, Liu Q, Yang J, Ma S, Frost RL (2012) The thermal behavior of kaolinite intercalation complexes-a review. Thermochim Acta 545:1–13. https://doi.org/10.1016/j.tca.2012.04.005

15. Zuo S, Sun X, Lv N, Qi C (2014) Rare earth-modified Kaolin/NaY-supported Pd–Pt bimetallic catalyst for the catalytic combustion of benzene. ACS Appl Mater Interfaces 6(15):11988–11996. https://doi.org/10.1021/am500138q

16. Yavuz Ö, Saka C (2013) Surface modification with cold plasma application on kaolin and its effects on the adsorption of methylene blue. Appl Clay Sci 85:96–102. https://doi.org/10.1016/j.clay.2013.09.011

17. Allen FJ, Truscott CL, Welbourn RJ, Clarke SM (2018) Anionic surfactant induced desorption of a cationic surfactant from mica. Appl Clay Sci 160:276–281. https://doi.org/10.1016/j.clay.2018.02.010

18. Ahmad HM, Kamal MS, Al-Harthi MA (2018) Rheological and filtration properties of clay-polymer systems: impact of polymer structure. Appl Clay Sci 160:226–237. https://doi.org/10.1016/j.clay.2018.01.016

19. Potsi G, Ladavos AK, Petrakis D, Douvalis AP, Sanakis Y, Katsiotis MS, Papavassiliou G, Alhassan S, Gournis D, Rudolf P (2018) Iron-substituted cubic silsesquioxane pillared clays: synthesis, characterization and acid catalytic activity. J Colloid Interface Sci 510:395–406. https://doi.org/10.1016/j.jcis.2017.09.003

20. Li C, Zhang B, Luo P, Shi H, Li L, Gao Y, Lee CT, Zhang Z, Wu W-M (2019) Performance of a pilot-scale aquaponics system using hydroponics and immobilized biofilm treatment for water quality control. J Cleaner Prod 208:274–284. https://doi.org/10.1016/j.jclepro.2018.10.170

21. Vinayagam R, Quadras M, Varadavenkatesan T, Debraj D, Goveas LC, Samanth A, Balakrishnan D, Selvaraj R (2023) Magnetic activated carbon synthesized using rubber fig tree leaves for adsorptive removal of tetracycline from aqueous solutions. Environ Res 216:114775. https://doi.org/10.1016/j.envres.2022.114775

22. Selvaraj R, Prabhu D, Kumar PS, Rangasamy G, Murugesan G, Rajesh M, Goveas LC, Varadavenkatesan T, Samanth A, Balakrishnaraja R, Vinayagam R (2023) Adsorptive removal of tetracycline from aqueous solutions using magnetic Fe2O3 / activated carbon prepared from Cynometra ramiflora fruit waste.

Chemosphere 310:136892. https://doi.org/10.1016/j.chemosphere.2022.136892

23. Kansara K, Patel P, Shukla RK, Pandya A, Shanker R, Kumar A, Dhawan A (2018) Synthesis of biocompatible iron oxide nanoparticles as a drug delivery vehicle. Int J Nanomedicine 13:79–82. https://doi.org/10.2147/IJN.S178426

24. Orosco P, Ruiz MdC, González J (2014) Synthesis of cordierite by dolomite and kaolinitic clay chlorination. Study of the phase transformations and reaction mechanism. Powder Technol 267:111–118. https://doi.org/10.1016/j.powtec.2014.07.009

25. Wang L, Shi Y, Zhang H, Bai X, Wang Y, Ma T (2014) Iron oxide nanostructures as highly efficient heterogeneous catalysts for mesoscopic photovoltaics. J Mater Chem A 2(37):15279–15283. https://doi.org/10.1039/C4TA03727H

26. Scherrer P (1918) Estimation of the size and internal structure of colloidal particles by means of röntgen. Nachrichten von der Gesellschaft der Wissenschaften zu Göttingen, Mathematisch-Physikalische Klasse 2:96–100. http://eudml.org/doc/59018

27. Madejová J (2003) FTIR techniques in clay mineral studies. Vib Spectrosc 31(1):1–10. https://doi.org/10.1016/S0924-2031(02)00065-6

28. Lasheen M, El-Sherif IY, Sabry DY, El-Wakeel S, El-Shahat M (2016) Adsorption of heavy metals from aqueous solution by magnetite nanoparticles and magnetite-kaolinite nanocomposite: equilibrium, isotherm and kinetic study. Desalin Water Treat 57(37):17421–9. https://doi.org/10.1080/19443994.2015.1085446

29. Sarma G, Gupta SS, Bhattacharyya K (2019) Removal of hazardous basic dyes from aqueous solution by adsorption onto kaolinite and acid-treated kaolinite: kinetics, isotherm and mechanistic study. SN Appl Sci 1(3):211. https://doi.org/10.1007/s42452-019-0216-y

30. Hwang S, Umar A, Dar G, Kim S, Badran RI (2014) Synthesis and characterization of iron oxide nanoparticles for phenyl hydrazine sensor applications. Sens Lett 12(1):97–101. https://doi.org/10.1166/sl.2014.3224

31. Mirbagheri NS, Sabbaghi S (2018) A natural kaolin/γ-Fe2O3 composite as an efficient nano-adsorbent for removal of phenol from aqueous solutions. Microporous Mesoporous Mater 259:134–141. https://doi.org/10.1016/j.micromeso.2017.10.007

32. Arizavi A, Mirbagheri N, Hosseini Z, Chen P, Sabbaghi S (2020) Efficient removal of naphthalene from aqueous solutions using a nanoporous kaolin/Fe3O4 composite. J Environ Sci Technol 1–12. https://doi.org/10.1007/s13762-019-02521-1

33. Meng X, Xu Y, Sun X, Wang J, Xiong L, Du X, Mao S (2015) Graphene oxide sheets-induced growth of nanostructured Fe3O4 for a high-performance anode material of lithium ion batteries. J Mater Chem A 3(24):12938–12946. https://doi.org/10.1039/C5TA01617G

34. Wang H, Li M, Wang B, Wang M, Kurash I, Zhang X, Feng W (2016) Magnetic Fe3O4 nanoparticle catalyzed chemiluminescence for detection of nitric oxide in living cells. Anal Bioanal Chem 408(20):5479–5488. https://doi.org/10.1007/s00216-016-9646-1

35. Nguyen T, Lefrant S (1989) XPS study of SiO thin films and SiO-metal interfaces. J Phys: Condens Matter 1(31):5197. https://doi.org/10.1088/0953-8984/1/31/019

36. Djebaili K, Mekhalif Z, Boumaza A, Djelloul A (2015) XPS, FTIR, EDX, and XRD analysis of Al2O3 scales grown on PM2000 alloy. J Spectrosc 2015. https://doi.org/10.1155/2015/868109

37. Wang X, Liu Y, Arandiyan H, Yang H, Bai L, Mujtaba J, Wang Q, Liu S, Sun H (2016) Uniform Fe3O4 microflowers hierarchical structures assembled with porous nanoplates as superior anode materials for lithium-ion batteries. Appl Surf Sci 389:240–246. https://doi.org/10.1016/j.apsusc.2016.07.105

38. Somasekhara Reddy MC, Sivaramakrishna L, Varada Reddy A (2012) The use of an agricultural waste material, Jujuba seeds for the removal of anionic dye (Congo red) from aqueous medium. J Hazard Mater 203–204:118–127. https://doi.org/10.1016/j.jhazmat.2011.11.083

39. Lorenc-Grabowska E, Gryglewicz G (2007) Adsorption characteristics of Congo Red on coal-based mesoporous activated carbon. Dyes Pigm 74(1):34–40. https://doi.org/10.1016/j.dyepig.2006.01.027

40. Langmuir I (1918) The adsorption of gases on plane surfaces of glass, mica and platinum. J Am Chem Soc 40(9):1361–1403. https://doi.org/10.1021/ja02242a004

41. Hall KR, Eagleton LC, Acrivos A, Vermeulen T (1966) Pore-and solid-diffusion kinetics in fixed-bed adsorption under constant-pattern conditions. Ind Eng Chem Fundamen 5(2):212–223. https://doi.org/10.1021/i160018a011

42. Freundlich H (1907) Über die adsorption in lösungen. Z Phys Chem 57(1):385–470. https://doi.org/10.1515/zpch-1907-5723

43. Munagapati VS, Kim D-S (2017) Equilibrium isotherms, kinetics, and thermodynamics studies for congo red adsorption using calcium alginate beads impregnated with nano-goethite. Ecotoxicol Environ Saf 141:226–234. https://doi.org/10.1016/j.ecoenv.2017.03.036

44. Temkin MI (1940) Kinetics of ammonia synthesis on promoted iron catalysts. Acta physiochim URSS 12:327–356

45. Araújo CS, Almeida IL, Rezende HC, Marcionilio SM, Léon JJ, de Matos TN (2018) Elucidation of mechanism involved in adsorption of Pb (II) onto lobeira fruit (Solanum lycocarpum) using Langmuir, Freundlich and Temkin isotherms. Microchem J 137:348–354. https://doi.org/10.1016/j.microc.2017.11.009

46. Lagergren (1907) Zurtheorie der sogenannten adsorption gelösterstoffe. Zeitschr f Chem und Ind der Kolloide 2:15. https://doi.org/10.1007/BF01501332

47. Yu L, Xue W, Cui L, Xing W, Cao X, Li H (2014) Use of hydroxypropyl-β-cyclodextrin/polyethylene glycol 400, modified Fe3O4 nanoparticles for congo red removal. Int J Biol Macromol 64:233–239. https://doi.org/10.1016/j.ijbiomac.2013.12.009

48. Ho Y-S, McKay G (1999) Pseudo-second order model for sorption processes. Process Biochem 34(5):451–465. https://doi.org/10.1016/S0032-9592(98)00112-5

49. Ho Y-S (2006) Review of second-order models for adsorption systems. J Hazard Mater 136(3):681–689. https://doi.org/10.1016/j.jhazmat.2005.12.043

50. Weber WJ, Morris JC (1963) Kinetics of adsorption on carbon from solution. J Sanit Eng Div, Am Soc Civ Eng 89(2):31–60. https://doi.org/10.1061/JSEDAI.0000430

51. Nazari G, Abolghasemi H, Esmaieli M, Pouya ES (2016) Aqueous phase adsorption of cephalexin by walnut shell-based activated carbon: a fixed-bed column study. Appl Surf Sci 375:144–153. https://doi.org/10.1016/j.apsusc.2016.03.096

52. Jaycock MJ, Parfitt GD (1981) Chemistry of interfaces. Ellis Horwood Ltd, Chichester

53. Li Q, Yue Q-Y, Su Y, Gao B-Y, Sun H-J (2010) Equilibrium, thermodynamics and process design to minimize adsorbent amount for the adsorption of acid dyes onto cationic polymer-loaded bentonite. Chem Eng J 158(3):489–497. https://doi.org/10.1016/j.cej.2010.01.033

54. Gupta VK, Pathania D, Sharma S, Agarwal S, Singh P (2013) Remediation and recovery of methyl orange from aqueous solution onto acrylic acid grafted Ficus carica fiber: isotherms, kinetics and thermodynamics. J Mol Liq 177:325–334. https://doi.org/10.1016/j.molliq.2012.10.007

55. Agarwal S, Tyagi I, Gupta VK, Ghasemi N, Shahivand M, Ghasemi M (2016) Kinetics, equilibrium studies and thermodynamics of methylene blue adsorption on Ephedra strobilacea saw dust

and modified using phosphoric acid and zinc chloride. J Mol Liq 218:208–218. https://doi.org/10.1016/j.molliq.2016.02.073

56. Wo R, Li Q-L, Zhu C, Zhang Y, Qiao G-f, Lei K-y, Du P, Jiang W (2019) Preparation and characterization of functionalized metal–organic frameworks with core/shell magnetic particles (Fe3O4@ SiO2@ MOFs) for removal of congo red and methylene blue from water solution. J Chem Eng Data 64(6):2455–2463. https://doi.org/10.1021/acs.jced.8b01251

57. Yang L, Zhang Y, Liu X, Jiang X, Zhang Z, Zhang T, Zhang L (2014) The investigation of synergistic and competitive interaction between dye Congo red and methyl blue on magnetic MnFe2O4. Chem Eng J 246:88–96. https://doi.org/10.1016/j.cej.2014.02.044

58. Yao Y, Miao S, Liu S, Ma LP, Sun H, Wang S (2012) Synthesis, characterization, and adsorption properties of magnetic Fe3O4@ graphene nanocomposite. Chem Eng J 184:326–332. https://doi.org/10.1016/j.cej.2011.12.017

59. Rahimi R, Kerdari H, RabbaniShafiee M (2011) Synthesis, characterization and adsorbing properties of hollow Zn-Fe2O4 nanospheres on removal of Congo red from aqueous solution. Desalination 280(1–3):412–418. https://doi.org/10.1016/j.desal.2011.04.073

60. Pandey G, Singh S, Hitkari G (2018) Synthesis and characterization of polyvinyl pyrrolidone (PVP)-coated Fe3O4 nanoparticles by chemical co-precipitation method and removal of Congo red dye by adsorption process. Int Nano Lett 8(2):111–121. https://doi.org/10.1007/s40089-018-0234-6

61. Kloster GA, Mosiewicki MA, Marcovich NE (2019) Chitosan/iron oxide nanocomposite films: effect of the composition and preparation methods on the adsorption of congo red. Carbohydr Polym 221:186–194. https://doi.org/10.1016/j.carbpol.2019.05.089

**Publisher's Note** Springer Nature remains neutral with regard to jurisdictional claims in published maps and institutional affiliations.